AUTOMATIC COMPUTER ANALYSIS OF DIGITAL DYNAMIC RADIONUCLIDE STUDIES OF THE CEREBRAL CIRCULATION

R. J. O'Reilly, R. E. M. Cooper, and P. M. Ronai

Institute of Medical and Veterinary Science, Adelaide, South Australia

Analog dynamic studies of the cerebral circulation performed with the scintillation camera and intravenously injected ^{99m}Tc-pertechnetate provide information on the vascularity of cerebral lesions and on the occlusion of major blood vessels (*1*). However, a large proportion of patients with clinical occlusive cerebrovascular disease have normal analog dynamic studies (*2–4*) suggesting that the technique is a relatively insensitive one. Limited success has been reported (*5*) for digital cerebral circulation studies.

Attempts in this laboratory to improve the sensitivity of cerebral dynamic studies by digital analysis have previously proved largely unsuccessful. Factors mitigating against success include (A) electronic noise in the data, (B) detector nonuniformity amounting to a ±10% variation in sensitivity from region to region of the gamma camera detector, (C) inaccuracy and nonreproducibility of regions of interest selected "by eyeball" from the CRT display of a data terminal or multiparameter analyzer, and (D) inequality of region-of-interest area due to observer error, asymmetry of the patient's head, or rotation of the patient's head under the detector.

This paper describes an empirical, completely automated, off-line computer analysis that has been designed to overcome all these possible sources of error.

METHOD

Recording. The patient is positioned supine with the orbitomeatal plane normal to the collimator surface and with the detector of the camera (Nuclear-Chicago Pho/Gamma III) above the patient's face. Approximately 12 mCi of ^{99m}Tc as pertechnetate in 0.5 ml saline are injected into the antecubital vein using a modified Oldendorf bolus-injection technique in which a tourniquet is used instead of a sphygmomanometer cuff. Standard premedication with $KClO_4$ is used as with the conventional brain scan.

The dynamic study is recorded digitally using dual analog-to-digital converters, a 1,600-channel multiparameter analyzer, and a seven-track magnetic-tape recorder (36 in./sec, 800 bpi) (*6*). It is simultaneously recorded in analog form on 35-mm film. Digital data are accumulated over a 40 × 40 element matrix for 1.8-sec intervals and serially dumped (in 0.35 sec) onto magnetic tape allowing 28 data blocks to be recorded over the 1 min of recording time.

Data from a uniform disk source of ^{99m}Tc are recorded on the tape prior to the first patient study of the day for subsequent correction of detector nonuniformity. Dynamic studies of 12–15 patients are recorded each day, and the tape is taken for analysis to the nearby University of Adelaide CDC 6400 computer at the end of the recording session.

Computer analysis. The computer carries out the following operations:

1. *Filtering.* Electronic noise is recorded as an abnormally high or low count. These counts are filtered out of all matrices in the following way.

The value of each matrix element (N) is compared with its four neighbors (a_i, i = 1–4). If it differs from all four neighbors by more than four standard deviations of the mean of the four neighbors, it is replaced by the mean.

Consider N and its 4 neighbors:

$$\begin{array}{ccc} & a_1 & \\ a_4 & N & a_2. \\ & a_3 & \end{array}$$

If for i = 1–4,

$$(N - a_i) > 4\left[\frac{\sum_{i=1}^{4} a_i}{4}\right]^{1/2}.$$

Replace N by

$$\sum_{i=1}^{4^4} \frac{a_i}{4}.$$

Received July 6, 1971; revision accepted Jan. 5, 1972.

For reprints contact: Peter M. Ronai, Director of Nuclear Medicine, The Institute of Medical and Veterinary Science, Box 14, Rundle St. Post Office, Adelaide, South Australia 5000.

2. *Smoothing.* To reduce statistical count variations, smoothing is performed using weighted spatial averaging (*7*). For the uniform disk source data, each element in the 40 × 40 matrix is replaced with a 13-element weighted spatial average in the following way.

The matrix

$$\begin{array}{ccccc} & & 1 & & \\ & 2 & 2 & 2 & \\ 1 & 2 & 5 & 2 & 1 \\ & 2 & 2 & 2 & \\ & & 1 & & \end{array}$$

is centered successively on each element of the flooded crystal data. (The numbers in each position of the smoothing matrix represent the weighting factors.) This matrix was empirically found to produce an isocount contour display of flooded crystal data consistent with that expected from the photomultiplier tube array in the detector.

3. *Nonuniformity correction* (*8*). Correction factors are determined for each of the 1,600 matrix elements using the uniform disk source data.

$$\text{C.F.} = m/a_i,$$

where C.F. is the correction factor for each of the 1,600 matrix elements, m the average count over all 1,600 matrix elements of uniform disk source data, and a_i the value of individual matrix elements of uniform disk source data.

4. *Region-of-interest selection.* The data blocks from each patient study are read in, filtered, corrected for detector nonuniformity, and written on a "scratch file". At the same time a cumulative sum of corresponding matrix elements in all 28 data blocks of each study is formed and retained in central memory. This forms the best available "image" of the head blood pool. This summed "image" is filtered and lightly smoothed with a five-element weighted spatial average.

$$\begin{array}{ccc} & 1 & \\ 1 & 2 & 1 \\ & 1 & \end{array}$$

is centered successively on each element of the summed head blood pool matrix. (The numbers in each position of the smoothing matrix represent the weighting factors.)

To determine the regions corresponding to the

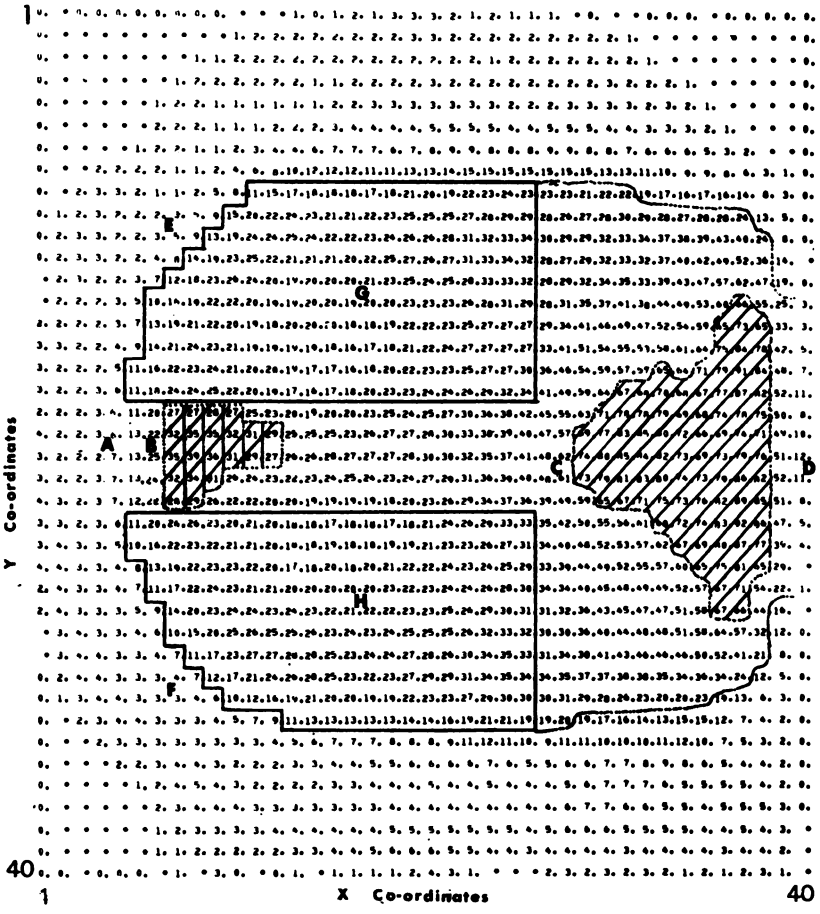

FIG. 1. Cumulative digital image of head smoothed, filtered, and normalized to maximum of 99 for printout by computer line printer. A, vertex; B, superior sagittal sinus; C, nasopharynx and major blood vessels; D, neck; E and F, step functions x_1 and x_j defining the calvarium; G, right hemicranium; H, left hemicranium.

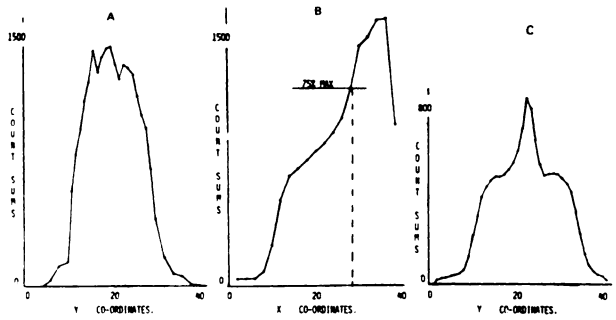

FIG. 2. Computer plot of: A, whole-row sums vs y coordinates. B, whole-column sums vs x coordinate. Plots A and B discriminate anatomical structures poorly. C, part-row sums vs y coordinates; superior sagittal sinus and lateral borders of head become apparent.

two hemicrania, the following series of operations is carried out on the cumulative digital "image" of the patient's head (Fig. 1):

a. Exclusion of nasopharynx. An arbitrary boundary is drawn between the brain and the nasopharynx by summing columns and taking the boundary at 75% of the maximum column sum (Fig. 2B).

b. Preliminary delineation of lateral boundaries of the superior sagittal sinus (SSS). Row sums are computed up to the 75% boundary. When plotted against the y coordinate, these part-row sums form a transverse profile of the head (Fig. 3) from which the lateral boundaries of the SSS (A and B in Fig. 3) and of the head (C and D in Fig. 3) can be selected. By computing sums only up to the 75% boundary, the irrelevant activity in the nasopharynx is excluded and the SSS is more clearly seen on the profile (Fig. 2A,C). Experience has shown that the SSS is either four or five rows wide. The decision between four and five is made by applying the following statistical test.

The five greatest part-row sums are ordered in descending order of magnitude S_1 through S_5. The mean of the second- and third-highest sums $[(S_2 + S_3)/2 = M_{2,3}]$ and the difference between the fourth and fifth $(S_4 - S_5 = d_{4,5})$ are evaluated. If $d_{4,5} \geqq 3(M_{2,3} - S_4)^{1/2}$ only four rows are included because it is considered improbable that S_5 belongs to the same group as $S_1 - S_4$. Otherwise five rows are included.

c. Delineation of lateral boundaries of the head. These are determined from the transverse profile (Fig. 3) derived in the preceding section by finding the first part-row sum at the right boundary of the head greater than 20% of the maximum part-row sum in the profile and then matching this with its closest part-row sum counterpart at the left boundary of the head.

d. Refining of lateral boundaries of the superior sagittal sinus. In the presence of abnormal blood pools due to tumors or infarcts in one or the other hemisphere, the peak corresponding to the SSS may be spuriously broadened (Fig. 4). This eventuality is allowed for by the next portion of the program which replots a

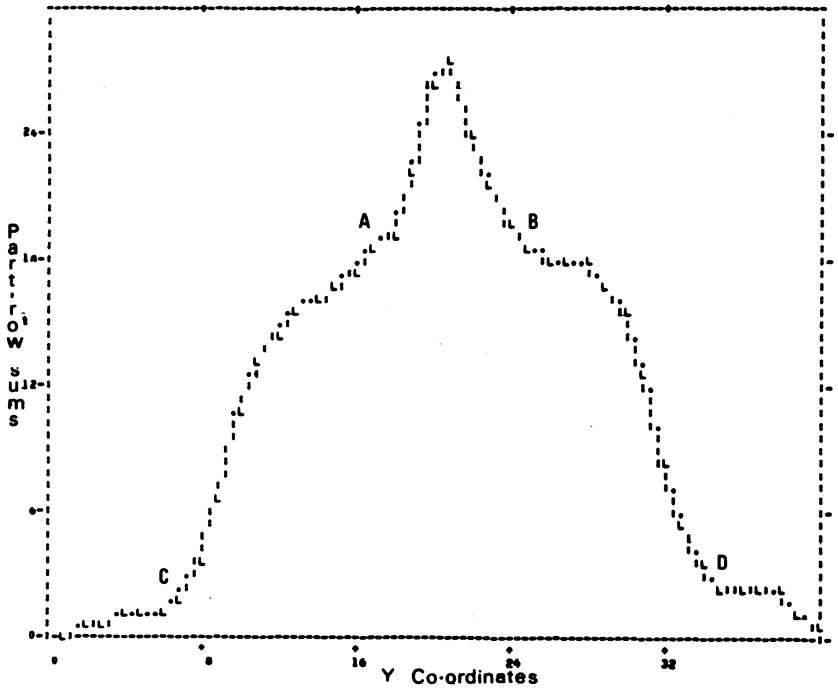

FIG. 3. Computer plot of part-row sums. A and B, lateral boundaries of superior sagittal sinus; C and D, right and left lateral head boundaries.

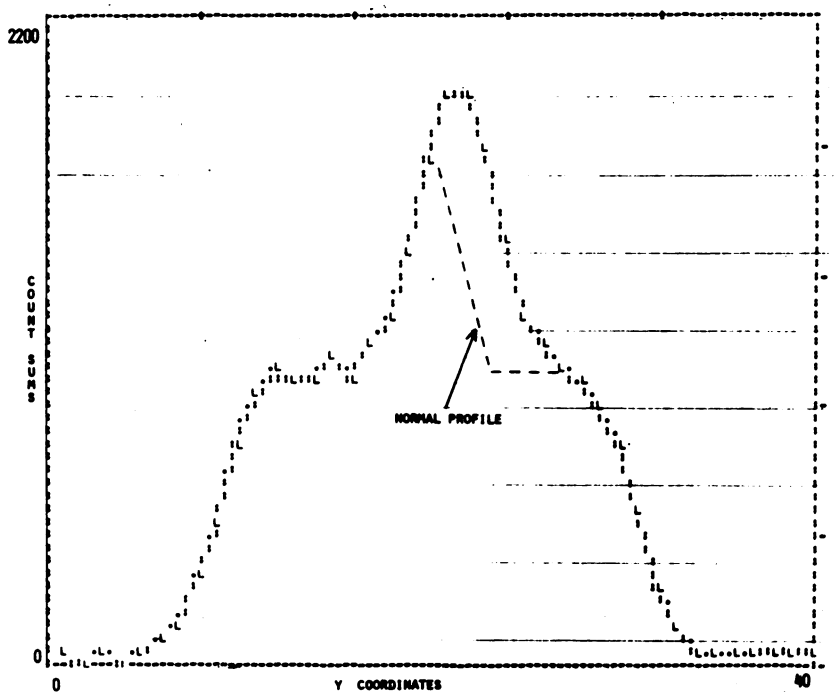

FIG. 4. Computer plot of transverse profile of patient with abnormal blood pool adjacent to superior sagittal sinus. Peak is higher and displaced to right of normal plot.

longitudinal profile similar to that in Fig. 2B except on this occasion it is plotted from sums of only those part-columns between the two lateral boundaries of the SSS initially determined in the above. The longitudinal profile from the patient with a left hemisphere tumor whose transverse profile was shown in Fig. 4 is seen in Fig. 5. The tumor blood pool is seen as a secondary peak (A in Fig. 5) to the right of (caudal to) the SSS peak. The first minimum (C in Fig. 5) after the first peak (B in Fig. 5) is found, and a new boundary is drawn at this minimum to replace the original 75% boundary. Part-row sums are then recomputed up to this new boundary and from these a transverse profile is plotted which clearly delineates the SSS with no interference from either the nasopharynx or abnormalities in the hemispheres. The statistical test described above in Paragraph b is then

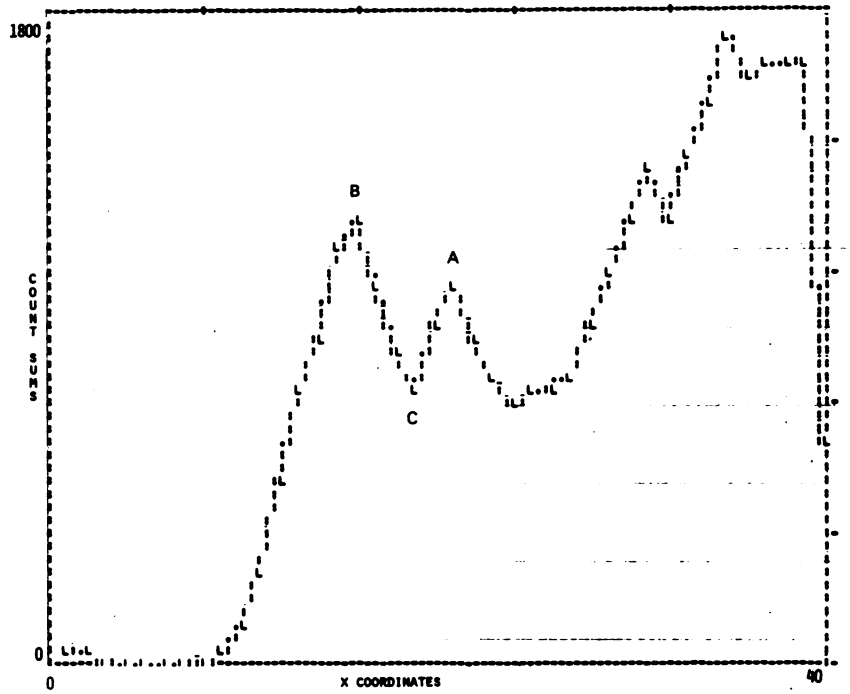

FIG. 5. Computer plot of longitudinal profile of patient with abnormal blood pool peak, A; adjacent to superior sagittal sinus peak, B; resulting in minimum, C.

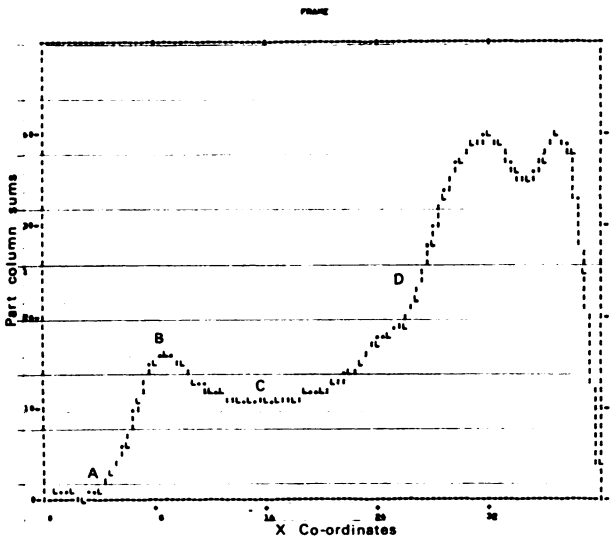

FIG. 6. Computer plot of part-column sums. A, vertex; B, superior sagittal sinus peak; C, depression corresponding to interhemispheric space; D, nasopharynx and major blood vessels.

reapplied to determine finally the lateral boundaries of the SSS.

e. Refining of boundary between brain and nasopharynx. A last longitudinal profile (Fig. 6) is generated from part-column sums obtained by summing columns only between the final lateral boundaries of the SSS determined in Paragraph d. By summing in this narrow midline strip, the boundary between brain and nasopharynx can be sensitively determined as the first significant rise (D in Fig. 6) after the trough (C in Fig. 6) caudal to the SSS peak (B in Fig. 6). This is again determined statistically as follows.

The minimum sum between the first significant (SSS) peak and the maximum (nasopharynx) peak is found. The five next lowest adjacent sums are found and the mean of these six values calculated (M_6). The boundary between brain and nasopharynx is defined as the first part-column sum less than $M_6 + 4(M_6)^{1/2}$ (i.e., the first significant rise above the minimum). The boundary is reevaluated using $M_6 + 3(M_6)^{1/2}$ if this boundary is more than 23 columns from the top of the head as determined below in Paragraph f.

f. Defining the peripheral boundaries of the head. The top of the head (A in Fig. 6) is defined from the longitudinal profile generated in e as the first part-column sum greater than 10% of the maximum part-column sum. The broad arc of the calvarium is defined as a step function between the two lateral boundaries of the head as determined in c by scanning each row and finding the first element in the row greater than 10% of the maximum element in the head.

g. Region-of-interest borders. The left and right regions of interest are now specified by the appropriate lateral boundary of the SSS as determined in d, the boundary between brain and nasopharynx as determined in e, the lateral boundary of the head as determined in c, and the curve of the calvarium and the top of the head as determined in f.

Region-of-interest normalization. Anatomical asymmetry of the head or rotation of the patient's head can result in the area of one region of interest being greater than the other. Differences of up to 25% are occasionally obtained from these causes. These effects can introduce spurious asymmetries in perfusion curves generated by spatial integration over such regions, and it is therefore necessary to normalize integrated counts registered in the two regions by the factors $(A_R + A_L)/2A_R$ for the right region of interest (A_R) and $(A_R + A_L)/2A_L$ for the left region of interest (A_L).

Compiling and plotting of histograms. The two regions of interest determined as above for a given patient are superimposed on each of the 28 1.8-sec frames of that patient's dynamic study, which are now read off the "scratch file". Counts are integrated over each region of interest and the sums normalized as discussed in "Region-of-interest normalization" (see above). This is done for all 28 frames and the resulting count sums are plotted on the same set of axes (Fig. 7) using a "Quickplot" routine (9) which produces a simulated graphic output on a line printer.

To improve the sensitivity of the "Quickplot" graph, the L:R ratio is evaluated at each data point and (after being suitably scaled to obtain a "normal" distribution of ratios about a mean of 1.00) is printed directly under the relevant data point on the plot.*

Computer printout. The uniform disk source data and the summed (blood pool) head data are each printed out as a 40 × 40 matrix of numbers enabling the counts recorded in each element to be checked. In addition, the data of Figs. 2B and 3–6 are printed out as well as the coordinates of the two chosen regions of interest, area-normalization factors, and patient-identification data. By printing out all these data a quick check can be made of any

* We have subsequently adopted an alternative procedure of printing the difference between L and R expressed in standard deviations.

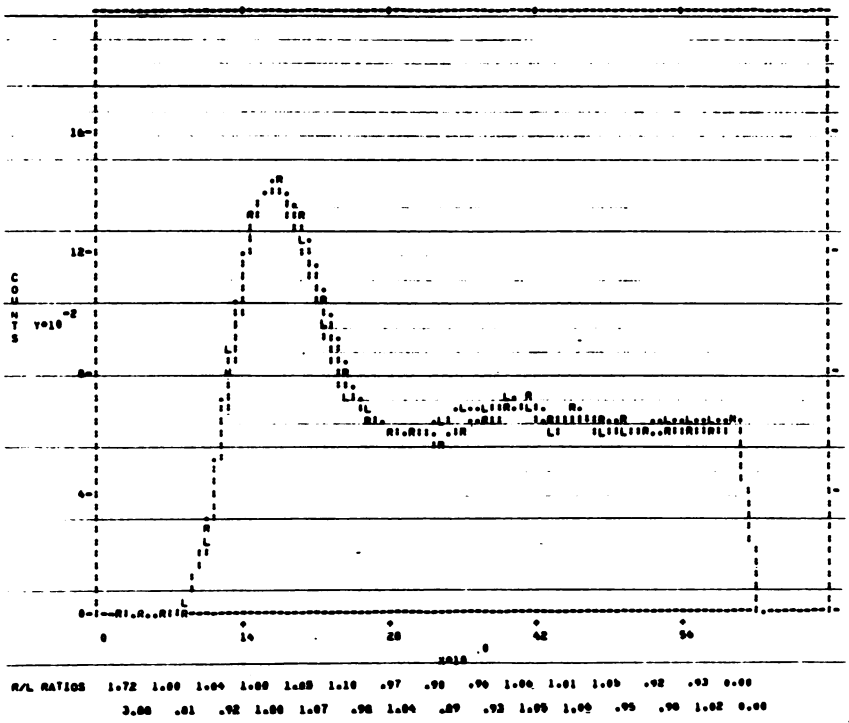

FIG. 7. Computer plot of normal cerebral circulation histogram with complete analysis. R and L, total counts/1.8 sec for right and left hemicrania, respectively. (Ratios are printed directly under each data point.)

stage of the program to ensure meaningful results.

The computer analysis is regularly available within 2 hr of completion of the recording session. Average central and peripheral processing times are 25 and 37 sec/patient, respectively, resulting in a processing cost of approximately $2.80 Australian (U.S. $3.10) for each study.

RESULTS

Figure 7 is a normal cerebral circulation histogram produced by the described technique from a patient without clinical evidence of occlusive cerebrovascular disease. In the ascending phase of the histogram, there is a variation in ratios from 0.92 to 1.04 and in the descending phase from 0.98 to 1.10. (The

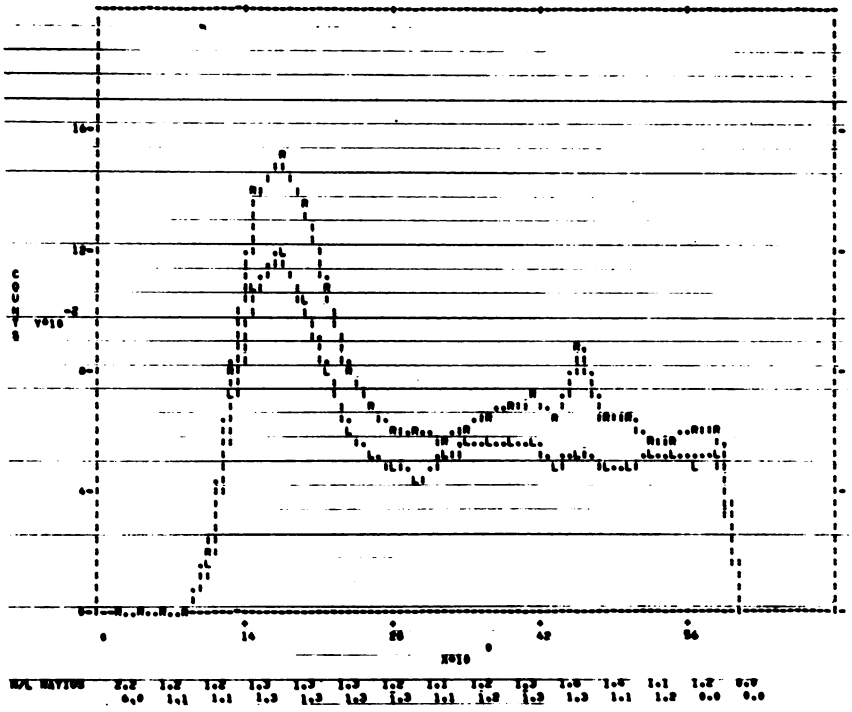

FIG. 8. Computer plot of cerebral circulation histogram of same patient as in Fig. 7 with no region-of-interest normalization or noise filtration. Latter is responsible for noise spike at 50-sec time point.

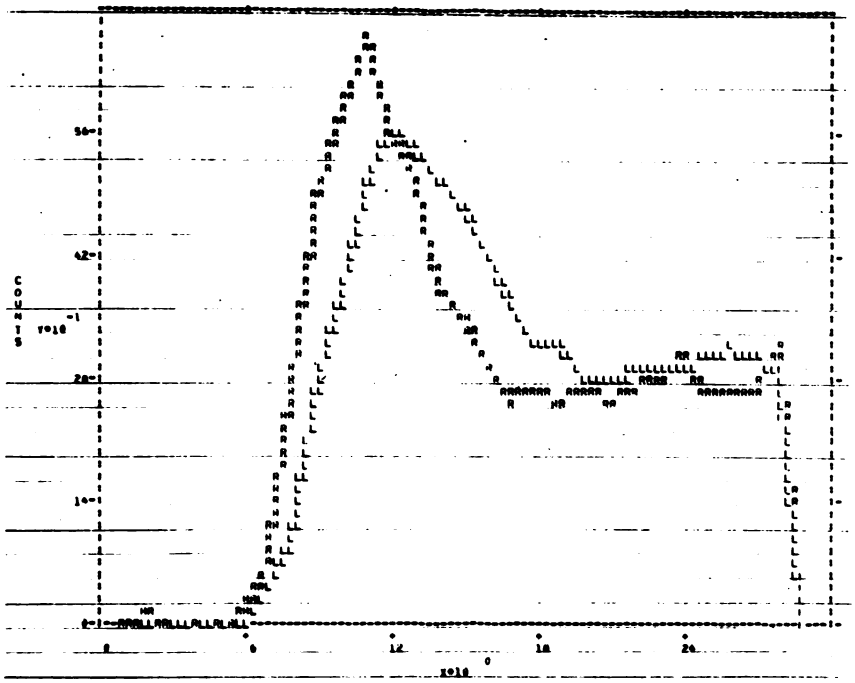

FIG. 9. Cerebral circulation histogram of patient with left internal carotid occlusion. There is marked delay and decrease in plot for left hemicranium.

ratios under the first four time points are statistically invalid.) These variations are considered to be within normal limits. The values of the ratios must be consistently outside the range (0.90 through 1.10) for each phase before the histogram is considered abnormal.

The digital analysis is able to compensate for poor alignment of the patient's head under the detector. In the case of the histogram shown in Fig. 7, the patient's head was incorrectly aligned, the sagittal plane being at a slight angle to the vertical. Figure 8, an example of the misleading results that can be obtained with unrefined programs, is the same data analyzed by a computer program which did not normalize data to the average region-of-interest area, resulting in a grossly abnormal plot. (This particular program also did not filter out false counts due to noise signals and a noise spike is seen at the 50-sec time point.)

Figure 9 is an example of the grossly abnormal digital dynamic study of a patient with a left internal carotid occlusion who presented with a right hemi-

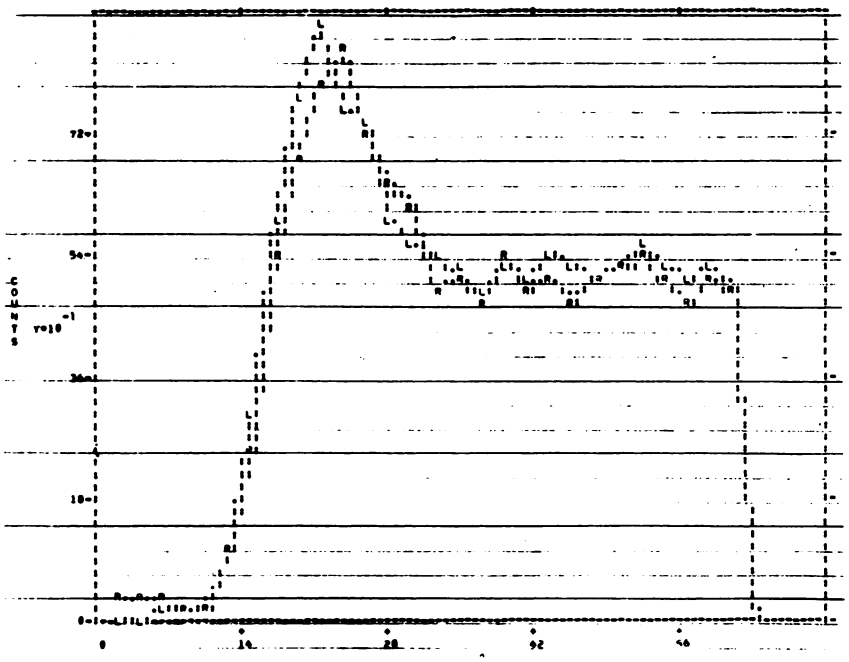

FIG. 10. Cerebral circulation histogram of patient with right transient ischemia. There is slight but definite delay in plot for right hemicranium.

plegia. The curve for the left hemicranium is markedly delayed and decreased with respect to the right. Figure 10 is a more subtle abnormality in a patient with a history of transient ischemic attacks of the left side of the body who had no clinical signs at the time of the investigation. There is a slight but definite delay in the curve for the right hemicranium with respect to the left which is not seen in the simultaneously recorded analog study (Fig. 11).

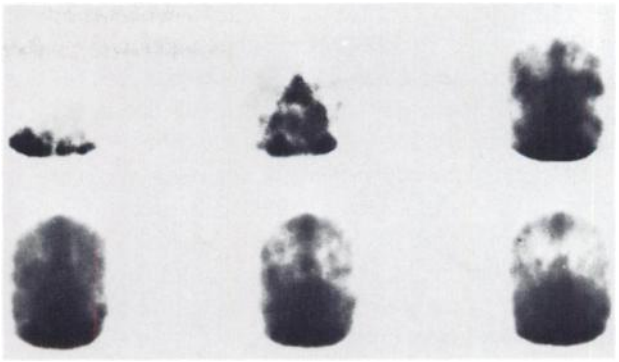

FIG. 11. Analog study recorded at same time as digital study of Fig. 10. Sequence of exposures is from top left to right, then bottom left to right. Each exposure was 4 sec. No asymmetry of hemispheric perfusion is discernible.

DISCUSSION

The use of this automated analysis of cerebral dynamic radionuclide data has several advantages:

1. It involves no commitment in time or effort by staff other than that involved in taking the tape to the computer (in our case a 5-min walk). The method thus lends itself to heavy-workload situations and is in fact part of the routine service in our laboratory where up to 15 patients are studied in this way every morning.
2. It avoids the extremely tedious task of manually selecting regions of interest in a large number of patients.
3. It selects regions of interest according to statistical criteria resulting in absolutely reproducible region-of-interest coordinates, a result which is difficult to achieve by manual selection. Further, it does this without sacrificing individualization of region-of-interest selection, as it allows all operations to be tailored to each patient's anatomical characteristics as well as taking into account the presence of abnormal blood pools.
4. It facilitates the implementation of correction and normalization procedures such as non-uniformity correction and region-of-interest normalization as well as various filtering and smoothing operations all of which proceed without human intervention.

Although the computer is designed to make allowances for abnormal vascular pools, gross lesions which show radionuclide concentration greater than that in the SSS may still cause the analysis to be aborted. It would be possible to modify the program to take even this eventuality into account but in practice the situation is always very obvious on the analog display. The main function of the digital analysis is to aid in the detection of minor abnormalities where the analog study is marginally abnormal or even normal (Figs. 10 and 11).

By limiting the analysis to a comparison of the two curves, the conclusions are independent of (A) the fact that an unknown fraction of the dose enters the cerebral circulation and (B) the fact that the shape of the bolus varies from study to study, and relatively independent of (C) the fact that the deadtime of the data-acquisition system is not zero and results in a variable percentage deadtime loss with varying counting rate.

This last problem is not nearly as significant in cerebral dynamic perfusion studies where counting rates are low as in cardiac dynamic perfusion studies where counting rates are high.

Considerable effort has been expended in attempting to assess the significance of various parameters of the perfusion curves: time from injection to peak, 95% rise time, transit time, timing of the peak for one region of interest compared with that for the other, maximum amplitude of the peak for one region of interest compared with that for the other, and finally, comparison of the slope of the ascending (arterial) phase of the curve for one region of interest compared with that of the other. Several of these parameters correlated with injected dose and with age in a population analysis (*3,4*), but in individual patients the presence of cerebrovascular disease correlated only with the last parameter—the comparison of the slopes of the ascending phase of the curve. Furthermore, this was the only reproducible parameter specifically related to cerebrovascular disease when studies were repeated in the same patient. In general, relative measurements between the left and right curves were highly reproducible when studies were repeated in the same patient, but as anticipated, absolute measurements of time and amplitude were not, due to the variability of the intravenous bolus. Difference in peak amplitudes, difference in transit times, and difference in height of the curves from the peak onwards correlated more closely with the presence of abnormal vascular pools such as in subdural hematoma, AV malformation, or vascular tumor. The "railroad pattern" in which the two curves

ascend together but are separated in the descending portion of the curves is particularly commonly seen in subdural hematoma. The clinical results of this program will be presented in more detail in a subsequent communication.

One problem which has not yet been overcome is the fact that the selected regions of interest include both internal and external carotid territory. The programming of regions of interest which exclude the calvarium to minimize the external carotid contribution is now being undertaken.

SUMMARY

This paper describes an empirical technique for automated off-line computer analysis of dynamic radionuclide studies of the cerebral circulation using a scintillation camera and associated digital data-acquisition equipment. The computer program carries out the following functions: (A) filtering and smoothing; (B) correction for nonuniform sensitivity of the gamma camera detector; (C) automatic selection of regions of interest corresponding to the cerebral hemispheres and avoiding the SSS, nasopharynx, and vascular structures at the base of the skull and neck (but including the calvarium with its external carotid blood supply); (D) normalization of data to the average region-of-interest area to correct for head asymmetry or rotation; and (E) plotting of histograms of total corrected counts/normalized region of interest/unit time, together with printout of L:R ratio at each data point.

The use of an automated analysis is ideally suited to high workload situations and the accuracy and speed of analysis are far greater than with the unsophisticated manual methods previously used. Individualized region-of-interest selection for each patient is preserved and at the same time the use of statistical criteria as a basis for region-of-interest selection results in absolutely reproducible regions of interest in a given patient. The program is an iterative one and can avoid abnormal blood pools in locating anatomical vascular landmarks during region-of-interest selection. The results of digital analysis using this technique have proved more sensitive in the detection of unilateral occlusive cerebrovascular disease than simultaneously recorded analog data.

REFERENCES

1. POWELL MR, ANGER HO: Blood flow visualization with the scintillation camera. *J Nucl Med* 7: 729–732, 1966

2. ROSENTHALL L, MARTIN RH: Cerebral transit of pertechnetate given intravenously. *Radiology* 94: 521–527, 1970

3. BURKE G, HALKO A: Cerebral blood flow studies with sodium pertechnetate Tc99m and the scintillation camera. *JAMA* 204: 319–324, 1968

4. OLDENDORF WH, KITANO M: Isotope study of brain blood turnover in vascular disease. *Arch Neurol* 12: 30–38, 1965

5. JACKSON GL, BLOSSER N: Nondestructive method for measuring cerebral hemispheric blood flow—a preliminary report using a gamma camera. *J Nucl Med* 10: 501–507, 1969

6. LOKEN MK, LINNEMANN RE, KUSH GS: Evaluation of renal function using a scintillation camera and computer. *Radiology* 93: 85–94, 1969

7. MACINTYRE WJ, CHRISTIE JH: A comparison of data averaging of radioisotope scan data by photographic and dimensional computer techniques. In *Medical Radioisotope Scintigraphy*, vol 1, Vienna, IAEA, 1969, pp 771–782

8. ANGER HO: In Discussion of Adams WE, Schenck P, Kampmann H, et al: Investigation of cardiac dynamics using scintillation camera and computer. In *Medical Radioisotope Scintigraphy*, vol 2, Vienna, IAEA, 1969, pp 77–91

9. HUDSON RH, MASTERS G, ROSS D: Subroutine Q4 CSIR quickplot. In Internal publication, C.S.I.R.O., Australia, Division of Computing Research, June 1966